Appl. Phys. A 83, 235–238 (2006)
DOI: 10.1007/s00339-006-3513-4

Applied Physics A
Materials Science & Processing

A.R. WOLL[1,✉]
J. MASS[2,3]
C. BISULCA[2]
R. HUANG[1]
D.H. BILDERBACK[1,4]
S. GRUNER[1,5]
N. GAO[6]

Development of confocal X-ray fluorescence (XRF) microscopy at the Cornell high energy synchrotron source

[1] Cornell High Energy Synchrotron Source, Cornell University, Ithaca, NY, USA
[2] University of Delaware, Newark, DE, USA
[3] Winterthur Museum, Garden and Library, Winterthur, DE, USA
[4] School of Applied and Engineering Physics, Cornell University, Ithaca, NY, USA
[5] Dept. of Physics, Cornell University, Ithaca, NY, USA
[6] X-ray Optical Systems, Albany, NY, USA

Received: 5 December 2005/Accepted: 12 December 2005
Published online: 1 March 2006 •

ABSTRACT A confocal X-ray fluorescence microscope was built at the Cornell High Energy Synchrotron Source (CHESS) to obtain compositional depth profiles of historic paintings. The microscope consists of a single-bounce, borosilicate monocapillary optic to focus the incident beam onto the painting and a commercial borosilicate polycapillary lens to collect the fluorescent X-rays. The resolution of the microscope was measured by scanning a variety of thin metal films through this confocal volume while monitoring the fluorescence signal. The capabilities of the technique were then probed using test paint microstructures with up to four distinct layers, each having a thickness in the range of 10–80 microns. Results from confocal XRF were compared with those from stand-alone XRF and visible light microscopy of the paint cross-sections. A large area, high-resolution scanner is currently being built to perform 3D scans on moderately sized paintings.

PACS 29.30.Kv; 68.37.Yz; 41.50.+h

1 Introduction

The composition of buried layers in a painting can often answer questions regarding the work's authenticity, the extent of previous restorations, the working methods of the artist, and the piece's condition. The most common technique for characterizing layered paint structures in works of art is scanning electron microscopy-energy dispersive spectroscopy (SEM-EDS) [1, 2]. While powerful, this technique requires a sample to be extracted from the painting. Typically, only a limited number of samples may be taken, especially from areas of greatest interest, such as the subject of a portrait. Although there are many non-destructive alternatives to SEM-EDS, such as neutron autoradiography (NA), X-ray fluorescence (XRF), proton-induced X-ray emission (PIXE), and infrared reflectivity, none reveal both the composition of individual layers as well as their position. During the past several years, improvements to X-ray optics based on hollow glass capillary tubes [3, 4] have enabled a new solution to the problem of non-destructive compositional analysis. The approach, called confocal XRF (CXRF) [5–8], is illustrated in Fig. 1. One optic focuses the incident beam, while the other, placed perpendicularly to the first, gathers fluorescence only from the region of the sample where the focal cone of the second optic intersects that of the first. To obtain the composition as a function of depth, the sample is scanned through this confocal volume.

Among the many types of X-ray optics, polycapillary lenses, consisting of a tapered bundle of thousands of hollow glass tubes, [3, 9] are uniquely well suited for collecting fluorescence from a point source. Because of this, all demonstrations of CXRF to date have used polycapillaries as the collecting optic [5–8]. In contrast, if the incident beam has a low divergence, as in the case of synchrotron radiation, other types of X-ray optics may be used as the focusing optic. For instance, Vincze et al. [8] used a compound refractive lens to achieve a smaller spot size and larger working distance than can be obtained with a polycapillary. In this article, we present the first results from a confocal microscope using a single-bounce monocapillary as the excitation optic. Monocapillaries are compact, have working distances up to several cm, and have reflection efficiencies of upwards of 90%. They have also been demonstrated to function well at up to 40 keV [10]. All of these characteristics make them attractive for CXRF.

One of the most promising features of CXRF is the possibility of extracting not just the locations of different elements in a sample, but also their concentrations. In traditional XRF, absorption of fluorescent X-rays by the sample, so-called matrix effects, prevents detailed modeling of fluorescence data for most samples [2]. With CXRF, one can first determine the elemental concentration of the outermost layer in a sample, then calculate the effect of absorption by that layer on the fluorescence intensity from buried layers. Recently, Vekemans et al. [8, 11] demonstrated one such technique. Here, we illustrate another method of analyzing CXRF data which, in some cases, gives the position and thickness of buried layers more precisely than the nominal, instrumental resolution. The technique explicitly accounts for the energy-dependent resolution of the microscope, and is applicable for layered structures in

✉ Fax: 607-255-9001, E-mail: aw30@cornell.edu

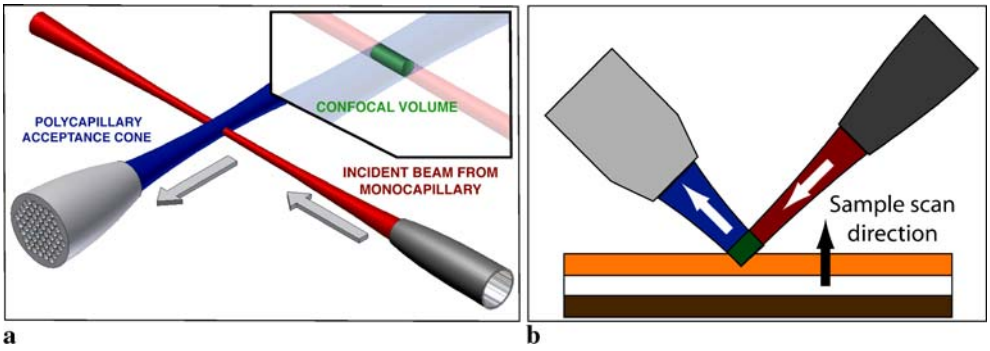

FIGURE 1 (**a**) Three-dimensional schematic view of the optical arrangement for the CHESS confocal XRF microscope. A single-bounce monocapillary focuses the incident beam, while a polycapillary collects fluorescence. (**b**) Side-view indicating the sample motion when performing a depth scan. As pictured, only fluorescence from the first layer will be detected

which the thickness T varies slowly with lateral dimension x, i.e. $\mathrm{d}T/\mathrm{d}x \ll 1$.

2 Experimental

2.1 *Microscope design*

The confocal XRF experiments were carried out at CHESS station D1, using monochromatic radiation at 16 keV, selected using a 1% bandpass multilayer monochromator with a d-spacing of 25.5 Å. A single-bounce monocapillary (#Pb605), developed at CHESS [4], was used to provide a focused incident beam of approximately 20 μm in diameter, while a double-focusing polycapillary lens with an input acceptance angle of 15.4°, on loan from X-ray Optical Systems (Albany, NY), was used to collect X-ray fluorescence from the sample. The unattenuated flux at the sample was estimated to be $\approx 2 \times 10^{11}$ photons/s, based on an unfocussed flux of 6×10^{11} photons/s/mm^2, the monocapillary reflection efficiency of $\approx 90\%$, and the area of the reflection surface perpendicular to the beam direction of 0.4 mm^2. For the data described below, a 1.6 mm thick aluminum block was used to attenuate the incident beam and prevent saturation of the detector. For depth-profiling, the sample is positioned with its surface normal 45° to the incident beam, and scanned as indicated in Fig. 1b. For alignment and scanning purposes, the monocapillary, sample, and polycapillary were all mounted on motorized translation stages. Fluorescence was collected by a Rontec (Carlisle, MA) Xflash silicon drift chamber placed behind the polycapillary, which has an energy resolution of approximately 0.17 keV at 6 keV, 5×10^4 counts/s.

2.2 *Sample preparation*

Two types of samples were prepared. The first were ≈ 0.5 μm films of Cu, Ti, and Au sputter-deposited onto glass slides. These films were used to measure the effective resolution at multiple fluorescence energies. The second set of samples consisted of multiple pigment layers made to mimic historic paint structures that have been modified with modern pigments, e.g. titanium white layered on top of lead white or vermillion. The pigments were obtained in powder form from Kremer Pigments, and characterized by X-ray fluorescence on a Rontec ArTAX spectrometer (Mo source, 20 keV, 300 μA, 100 s count time). Paints were prepared from each of these pigments by mixing 1 ml of pigment with 4 ml of a 20% v/v mixture of acrylic copolymer binder, Paraloid B-72 (Rohm and Haas), and acetone. Such paints were then brushed onto glass substrates and allowed to dry for 15–20 minutes before applying the next coat. Several coatings of each paint were applied in order to achieve a nominal layer thickness of at least 20 μm.

3 Modeling CXRF from layered samples

3.1 *Depth resolution*

To obtain the instrumental depth resolution, depth scans were performed on a series of Ti, Cu, and Au metal films, each approximately 0.5 μm thick. Each scan consists of N distinct fluorescence spectra, each corresponding to a different depth of the confocal volume relative to the film. The inset to Fig. 2 shows the integrated Ti K_α intensity from one such scan as a function of depth. The full width at half maximum (FWHM) of the peak is 43.5 μm, as determined from fitting to a Gaussian profile. Since this width is much larger than the film thickness, it corresponds to the depth resolution of the microscope at the Ti K_α energy of 4.51 keV. The main part of Fig. 2 shows FWHM for all the characteristic lines from scans of each of the three films. The depth resolution of the microscope ranges from 55 μm at 2 keV to 35 μm at 8 keV and above.

The energy dependence in Fig. 2 originates from the polycapillary, whose acceptance angle is determined by the critical

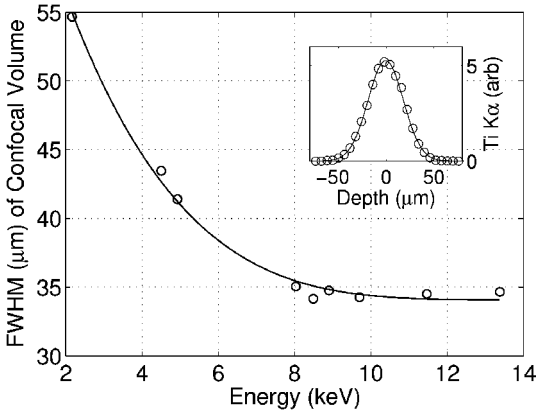

FIGURE 2 Full-width at half maximum (FWHM) of fluorescence intensity vs. depth from scans of thin (≈ 0.5 μm) titanium, copper and gold films, plotted as a function of fluorescence energy. Each film gives multiple data points corresponding to different emission lines. From lowest to highest energy, the data points correspond to: Au M_α, Ti K_α, K_β, Cu K_α, K_β Au L_α, L_β, L_γ, and L_ι [12]. *Inset* shows the Ti K_α depth scan as an example. The *solid line* is a 4th order polynomial fit to the measured values

angle for total external reflection [9]. The solid line in Fig. 2 is a 4th order polynomial fit to the data, constrained to be monotonically decreasing in the region of interest, and is used in the following section to estimate the resolution for fluorescence energies not represented in Fig. 2. Such an interpolation is justified by the smooth dependence of the critical angle on energy.

It should be noted that these depth scans are not completely described by a Gaussian function: the fits described above yield χ^2 values of ~ 2.5–3. Better fits ($\chi^2 \sim 1.2$–1.5) were obtained by adding a skew component to the model, which could indicate a slight asymmetry in either of the two optics – most likely the monocapillary. However, since there was no obvious, physical dependence of this component on fluorescence energy, it could not be estimated for energies other than those actually measured. Ideally, one would measure the resolution function for each element of interest.

3.2 *Multilayered paint sample*

Figure 3a shows an optical cross-section of one of the multilayered paint samples discussed in Sect. 2.2. The different pigments are indicated in the figure. A depth scan on this sample was performed, and clearly showed four distinct elemental constituents: cadmium, chromium, copper, and lead. Integrated intensities of the strongest fluorescence lines for each element are shown in Fig. 3b. The collection time for each point was 1 s, and the spectra were taken at 4 μm intervals.

The peaks in Fig. 3b are clearly offset from one another, indicating the four distinct layers in the film. However, due to the varying resolution of the microscope, the precise thickness of each layer cannot be trivially extracted from the raw data. For example, the FWHM of the cadmium L_α peak is ~ 50 μm, which is nearly identical to the resolution of the depth microscope at 3.13 keV as estimated from Fig. 2.

To accurately extract information about each layer in the sample, the data were fit to a simple model of intensity vs. depth. Each layer $L = 1...4$ is assumed to have a constant total density ϱ_L, comprised of elemental densities ϱ_n for each element n. The interfaces between layers are assumed to be sharp. Both the incident beam and fluorescence suffer absorption as they travel to and from a particular depth z in the layer, so that the intensity of a particular fluorescence line f from a thin volume of a layer can be written

$$I_{\mathrm{L,f}}(z) = A_{\mathrm{L,f}} \mathrm{e}^{-(z-z_1)\{\sqrt{2}\sum_n \varrho_n(\mu_n(E_\mathrm{o})+\mu_n(E_\mathrm{f}))\}}\,, \tag{1}$$

where z_1 corresponds to the top of the layer, and positive z corresponds to increasing depth. $I_{L,f}(z) = 0$ when $z < z_1$ or $z > z_2$, z_2 being the bottom interface. E_o and E_f are the energies of the incident and fluorescence beams, and the factor $\sqrt{2}$ arises from the 45° angle of both beams with respect to the surface normal. $A_{\mathrm{L,f}}$ is proportional to the incident flux and the density of the fluorescing element $\varrho_{\mathrm{L,f}}$, and also includes absorption by layers above the layer of interest. We assume that the lateral variation in layer thickness $T(x)$ is slowly varying, $\mathrm{d}T/\mathrm{d}x \ll 1$, so that $A_{\mathrm{L,f}}$ is constant. The sum is over all elements n in the layer, which each have their own absorption coefficients μ_n and densities ϱ_n. Equation (1) ignores secondary fluorescence, which is justified since the incident intensity is necessarily far larger than the fluorescence intensity within the confocal volume. If we write the term in curly braces in (1) as $\mu'_{L,f}$, then the intensity simplifies to:

$$I_{\mathrm{L,f}}(z) = A_{\mathrm{L,f}} \mathrm{e}^{-\mu'_{\mathrm{L,f}}(z-z_1)}\,, \quad z_1 < z < z_2\,. \tag{2}$$

Equation (2) constitutes a four-parameter model for fluorescence intensity vs. depth for a CXRF microscope with ideal depth resolution. For a real microscope, it must be convolved with the finite instrumental resolution function at energy E_f, as described in Sect. 3.1, to obtain the measured intensity vs. depth. If we denote this function $R_{E_\mathrm{f}}(z)$, then the detected

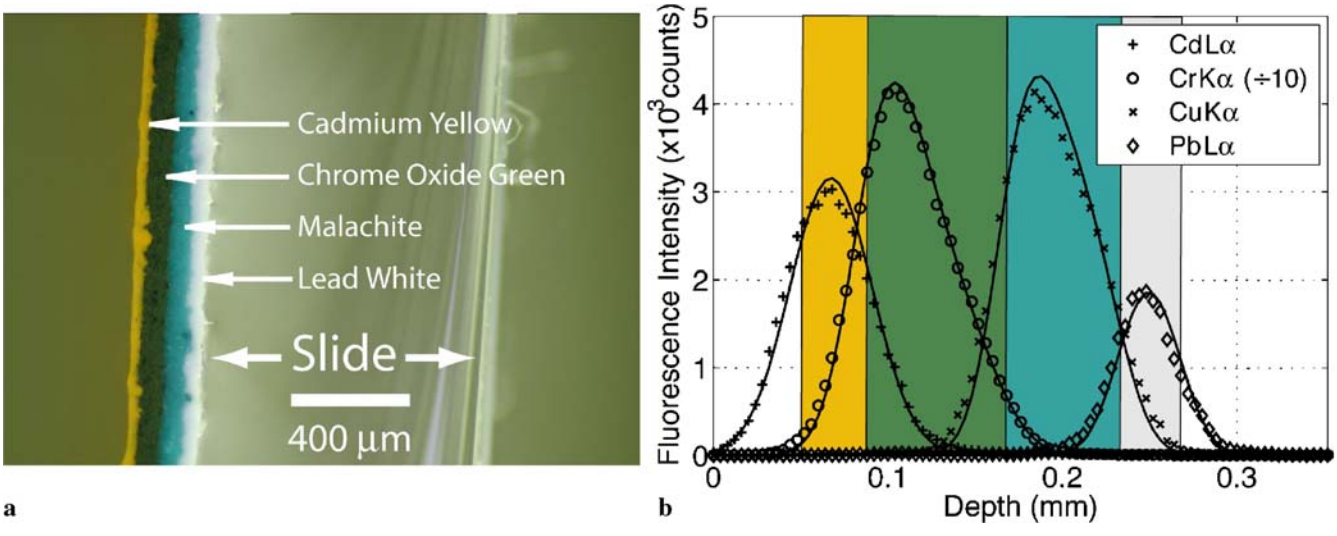

FIGURE 3 (**a**) Optical cross-section of a multilayered paint sample on a glass slide. The four pigments are indicated in the figure, and correspond to CdS (cadmium yellow), Cr_2O_3 (chromium oxide green), $Cu_2CO_3(OH)_2$ (malachite), and $2Pb(CO_3)Pb(OH_2)$ (lead white). (**b**) Intensity vs. depth of several particular fluorescence peaks, indicated in the *inset*, from a depth scan of the sample in (**a**). The Cr K_α data is rescaled for the plot, as indicated by the *inset*. The *solid lines* and *shaded regions* represent the best-fit curves and individual layer profiles as extracted from fits to the model described in the text

intensity $I_{\mathrm{D,f}}(z)$ when the confocal volume is centered on position z is written:

$$I_{\mathrm{D,f}}(z) = \int_{-\infty}^{\infty} I_{\mathrm{L,f}}(z)\, R_{E_\mathrm{f}}(z - z')\, \mathrm{d}z' \,. \tag{3}$$

To fit the data in Fig. 3b, the 126-point depth profiles for eight distinct fluorescence energies, two per layer, were combined into a single 1008-point data set. Equation (3) is applied to each of these eight spectra, and the difference between the model and data was minimized using a non-linear least squares algorithm. The functions $R_{E_\mathrm{f}}(z)$ are taken to be Gaussian profiles, $R_{E_\mathrm{f}}(z) \propto \exp(-z^2/2\,\sigma^2)$, whose widths σ are taken from the best-fit curve in Fig. 2 with $\sigma = \mathrm{FWHM}/2.35$. The $4 \times 8 = 32$ fit parameters are reduced to 21 by the fact that K_α and K_β pairs of the same elements share the same z_1 and z_2, and the assumption of non-overlapping interfaces, i.e. the bottom interface, z_2, of layer one coincides with the top interface, z_1, of layer two.

The solid lines in Fig. 3b correspond to best-fit intensity profiles from the fit to (3). The best-fit interface positions, the parameters z_1 and z_2 for each layer, are represented by the shaded areas, and correspond to layer thicknesses of 38 (cadmium yellow), 80 (chromium oxide green), 69 (malachite), and 34 (lead white) microns. These values are in excellent agreement with thicknesses obtained from the optical cross-section shown in Fig. 3a. The uncertainty in the best-fit positions of the interfaces is ± 5 μm to a confidence level of 70%. These uncertainties are far below the depth resolution values implied by Fig. 2, demonstrating the advantage of our approach.

The purpose of applying (3) was to extract precise information about layers that were already known to be distinct from simple inspection of the data in Fig. 3b. In real paintings, many paint layers are likely to be thinner than the layers in Fig. 3a, and/or compositionally similar to adjacent layers. For example, lead may be present in two adjacent layers but with different concentrations. In addition, the assumption that $\mathrm{d}T/\mathrm{d}x \ll 1$ may not hold. In such cases, application of (3) may be difficult or impossible, e.g. the fit may fail to converge. By far the most efficient way of addressing such difficulties is to improve the instrumental resolution. An improvement in resolution of a factor of 2–3 should be possible with current technology. However, the combination of the analysis shown here with other spectroscopic methods e.g. clustering [8], may provide additional means of resolving distinct layers under such conditions.

4 Summary

We have successfully demonstrated CXRF using the combination of a single-bounce monocapillary for the focusing optic and polycapillary as the collector. We have also described a semi-empirical model for CXRF data from simple, layered structures, and demonstrated its use on data from a four-layer paint structure on a glass slide. In the near future, we will commission a large-area, 3D scanner for the application of CXRF to large-scale paintings. The scanner has a range of $600 \times 700 \times 100\,\mathrm{mm}^3$, and can accommodate paintings up to $110 \times 140\,\mathrm{cm}^2$ when used in the D1 hutch at CHESS.

ACKNOWLEDGEMENTS This work is based upon research conducted at the Cornell High Energy Synchrotron Source (CHESS) which is supported by the National Science Foundation (NSF) and the National Institutes of Health/National Institute of General Medical Sciences under NSF award DMR 0225180. The confocal XRF work is supported by NSF award DMR 0415838.

The authors would like to thank Mark Bockrath, Richard Wolbers, and Joyce Hill Stoner for their helpful suggestions and discussions, and Mark Bockrath for the donation of his painting.

REFERENCES

1 W. Taft, J. Mayer, *The Science of Paintings* (Springer-Verlag, New York, 2000)
2 E. Ciliberto, G. Spoto, *Modern Analytical Methods in Art and Archaeology* (Wiley, New York, 2000)
3 M. Kumakhov, X-ray Spectrom. **29**, 343 (2000)
4 D. Bilerback, X-ray Spectrom. **32**, 195 (2003)
5 B. Kanngiesser, W. Malzer, I. Reiche, Nucl. Instrum. Methods B **211**, 259 (2003)
6 B. Kanngiesser, W. Malzer, A.F. Rodriguez, I. Reiche, Spectrochim. Acta B **60**, 41 (2005)
7 K. Janssens, K. Proost, G. Falkenberg, Spectrochim. Acta B **59**, 1637 (2004)
8 L. Vincze, B. Vekemans, F.E. Brenker, G. Falkenberg, K. Rickers, A. Somogyi, M. Kersten, F. Adams, Anal. Chem. **76**, 6786 (2004)
9 N. Gao, K. Janssens, In: *X-ray Spectrometry: Recent Technological Advances*, K. Tsuji, J. Injuk, R. Van Grieken (Eds.) (Wiley, West Sussex, 2004)
10 G. Falkenburg, K. Rickers, D.H. Bilderback, R. Huang, HASYLAB Annual report, http://www-hasylab.desy.de/science/annual_reports/2003_report/part1/intern/11062.pdf, last accessed March 30, 2005
11 B. Vekemans, L. Vincze, F.E. Brenker, F. Ada, J. Anal. At. Spectrosc. **19**, 1302 (2004)
12 J. Bearden, Rev. Mod. Phys. **39**, 78 (1967)